Inorg. Chem. **2005**, *44*, 3499–3511

Effect of 2-(2-Pyridyl)azole-Based Ancillary Ligands (L^{1-4}) on the Electrophilicity of the Nitrosyl Function in $[Ru^{II}(trpy)(L^{1-4})(NO)]^{3+}$ [trpy = 2,2′:6′,2″-Terpyridine]. Synthesis, Structures, and Spectroscopic, Electrochemical, and Kinetic Aspects

Nripen Chanda,[‡] Debamita Paul,[‡] Sanjib Kar,[‡] Shaikh M. Mobin,[‡] Anindya Datta,[‡] Vedavati G. Puranik,[§] K. Krishnamurthy Rao,[||] and Goutam Kumar Lahiri*[,‡]

Department of Chemistry and School of Biosciences and Engineering, Indian Institute of Technology—Bombay, Powai, Mumbai-400076, and Center For Materials Characterization, National Chemical Laboratory, Pune, Maharashtra-411008, India

Received December 23, 2004

Ruthenium nitrosyl complexes $[Ru(trpy)(L^{1-4})(NO)]^{3+}$ (**13**–**16**) [trpy = 2,2′:6′,2″-terpyridine, L^1 = 2-(2-pyridyl)-benzoxazole, L^2 = 2-(2-pyridyl)benzthiazole, L^3 = 2-(2-pyridyl)benzimidazole, L^4 = 1-methyl-2-(2-pyridyl)-1*H*-benzimidazole] were obtained in a stepwise manner starting from $[Ru^{II}(trpy)(L^{1-4})(Cl)]ClO_4$ (**1**–**4**) → $[Ru^{II}(trpy)(L^{1-4})(H_2O)](ClO_4)_2$ (**5**–**8**) → $[Ru^{II}(trpy)(L^{1-4})(NO_2)]ClO_4$ (**9**–**12**) → $[Ru^{II}(trpy)(L^{1,2,4})(NO)](ClO_4)_3$ (**13**, **14**, **16**)/$[Ru^{II}(trpy)(L^3)(NO)](ClO_4)_2(NO_3)$ (**15**). Crystal structures of **1**, **2**, **4**, **9**, **12**, **13**, **15**, and **16** established the stereoretentive nature of the transformation processes. Though the complexes of L^1, L^3, and L^4 were isolated in the isomeric form **A** (π-acceptor trpy and azole ring in the equatorial plane and the pyridine and chloride donors in the axial positions), complexes of L^2 preferentially stabilized in form **B** (trpy and pyridine in the equatorial plane and the azole ring and chloride donors in the axial positions). The ν(NO) stretching frequency varied in the range of 1957–1932 cm^{-1}, **13** ≫ **14** ≈ **15** > **16**, primarily depending on the electronic aspects of L as well as the isomeric structural forms. The coordinated nitrosyl function underwent successive reductions of $[Ru^{II}–NO^+]^{3+}$ → $[Ru^{II}–NO^•]^{2+}$ and $[Ru^{II}–NO^•]^{2+}$ → $[Ru^{II}–NO^-]^+$, and the first reduction potential follows the order **14** > **13** ≫ **15** ≈ **16**. The nearly axial EPR spectra having nitrogen hyperfine splittings (A ≈ 26 G) at 77 K of $\mathbf{13}^-$–$\mathbf{16}^-$ with $\langle g \rangle$ ≈ 2.0 established that the reduction process is largely centered around the nitrosyl function. Despite an appreciably high ν(NO), the complexes were found to be unusually stable even in the aqueous medium. They transformed slowly and only partially into the corresponding nitro derivatives in H_2O ($k \approx 10^{-4}$ s^{-1} and K = 0.4–3.8). The chloro (**1**–**4**), aqua (**5**–**8**), and nitro (**9**–**12**) derivatives displayed reasonably strong emissions near 700 nm at 77 K ($\phi = 10^{-1}$–10^{-2}). The aqua derivative **7** was found to interact with the calf thymus and the circular form of *p*-Bluescript SK DNA.

Introduction

There is an intense renewed interest in the area of nitrosyl chemistry primarily due to its wide range of applications in biological[1] and environmental[2] processes. By virtue of its unique redox noninnocent characteristic, it can shuttle between the three possible states NO^+, NO, and NO^-, particularly on coordination to a metal ion. The stability of a particular redox state of the NO molecule in a complex environment essentially depends on the electronic nature of the coligands associated with the metal nitrosyl fragment. For example, in metmyoglobin, the iron center binds with the NO as $Fe^{II}–NO^+$,[3] and in reduced vitamin B_{12}, the cobalt center binds with the NO in the form of $Co^{III}–NO^-$.[4] Moreover, the generation of a strongly electrophilic $M–NO^+$ moiety deserves special attention as the coordinated elec-

* Author to whom correspondence should be addressed. E-mail: lahiri@chem.iitb.ac.in.

[‡] Department of Chemistry, Indian Institute of Technology—Bombay.

[§] School of Biosciences and Engineering, Indian Institute of Technology—Bombay.

[||] National Chemical Laboratory.

10.1021/ic048184w CCC: $30.25
Published on Web 04/13/2005

trophilic NO^+ is known to undergo a variety of molecular transformations on nucleophilic attack.[5] The degree of electrophilicity of the coordinated $M-NO^+$ can be tuned via the modulation of the ancillary functions in the complex matrixes. Thus, a substantial variation of the ν(NO) frequency in a particular environment of $[(trpy)(L)Ru^{II}-NO]^{3+}$ (trpy = 2,2′:6′,2″-terpyridine) has been observed depending on the π-acidic and σ-donor strengths of L, and it follows the order L = 2-phenylazopyridine (pap) (1960 cm^{-1})[6] > 2,2′-bipyridine (bpy) (1952 cm^{-1})[7] > 2,2′-dipyridylamine (dpa) (1945 cm^{-1})[8] > acetylacetonate (acac) (1914 cm^{-1})[9] > 2-phenylpyridine (pp) (1858 cm^{-1}).[10] Therefore, it was considered worthwhile to introduce a new set of ancillary ligands with varying electronic nature in the (trpy)Ru−NO core which could facilitate (i) stabilization of a strongly electrophilic Ru−NO center and (ii) tuning of the electrophilicity of the Ru−NO moiety via the modulation of L. This situation has prompted the present program of investigating the selective introduction of pyridyl-based heterocycles, viz., 2-(2-pyridyl)azoles, as ancillary ligands (L^1-L^4) comprising a coordinating pyridyl ring on one side and an azole ring attached to O, S, NH, and NMe groups, respectively, on the other side to the Ru(trpy)Cl core. This approach resulted in the formation of a strongly electrophilic but stable nitrosyl derivative $\{(trpy)(L^1)Ru-NO\}$ (L^1 = 2-(2-pyridyl)benzoxazole) (**13**), and the nitrosyl functions in the complexes **13**−**16** [**14**, L^2 = 2-(2-pyridyl)benzthiazole; **15**, L^3 = 2-(2-pyridyl)benzimidazole; **16**, L^4 = 1-methyl-2-(2-pyridyl)-1*H*-benzimidazole] indeed show a variation in their ν(NO) frequencies (1957−1932 cm^{-1}) primarily based on the electronic aspects of L^{1-4} as well as their different geometrical structural forms.

The work presented in this paper describes the synthesis, structures, and spectroscopic and electrochemical aspects of the nitrosyl complexes **13**−**16**. The effectiveness of L^1-L^4 in the (trpy)Ru−NO core specifically toward the electrophilicity and stability of the coordinated NO function with special reference to earlier reported ancillary ligands is deliberated. It may be noted that to the best of our knowledge only a limited number of ruthenium 2-(2-pyridyl)azole (L^1-L^4) derivatives are known.[11]

Results and Discussion

The nitrosyl complexes **13**−**16** were prepared in a stepwise manner, $[Ru^{II}(trpy)(L^{1-4})(Cl)]ClO_4$ (**1**−**4**) → $[Ru^{II}(trpy)(L^{1-4})(H_2O)](ClO_4)_2$ (**5**−**8**) → $[Ru^{II}(trpy)(L^{1-4})(NO_2)]ClO_4$ (**9**−**12**) → $[Ru^{II}(trpy)(L^{1,2,4})(NO)](ClO_4)_3$ (**13**, **14**, **16**)/$[Ru^{II}(trpy)(L^3)(NO)](ClO_4)_2(NO_3)$ (**15**) (Scheme 1). The direct synthesis of the nitrosyl species **13**−**16** either from the chloro derivatives **1**−**4** or from the aqua complexes **5**−**8** by using NO gas was not successful. Therefore, the sequential synthetic methodologies were followed (Scheme 1). The ancillary functions L^1-L^4 in **1**−**16** are systematically bonded to the ruthenium ion via the azole (N^1) and pyridyl (N^2) nitrogen donor centers, forming a five-membered neutral chelate ring.

The neutral N^1 of the benzimidazole group of L^3 is preferentially functioning as a donor center[11b−f,12] in **3**, **7**, **11**, and **15**, though the deprotonated anionic nitrogen [N^-] of the benzimidazole group is also known to be a probable coordinating site.[13]

(1) (a) Howard, J. B.; Rees, D. C. *Chem. Rev.* **1996**, *96*, 2965. (b) Burgees, B. K.; Lowe, D. J. *Chem. Rev.* **1996**, *96*, 2983. (c) Eady, R. R. *Chem. Rev.* **1996**, *96*, 3013. (d) Stamler, J. S.; Singel, D. J.; Loscalzo, J. *Science* **1992**, *258*, 1898. (e) Pfeiffer, S.; Mayer, B.; Hemmens, B. *Angew. Chem., Int. Ed.* **1999**, *38*, 1714. (f) Lang, D. R.; Davis, J. A.; Lopes, L. G. F.; Ferro, A. A.; Vasconcellos, L. C. G.; Franco, D. W.; Tfouni, E.; Wieraszko, A.; Clarke, M. J. *Inorg. Chem.* **2000**, *39*, 2294. (g) Richter-Addo, G. B.; Legzdins, P.; Burstyn, J. *Chem. Rev.* **2002**, *102*, 4. (h) Moncada, S.; Palmer, R. M. J.; Higgs, E. A. *Pharmacol. Rev.* **1991**, *43*, 109. (i) Ritcher-Addo, G. B.; Legzdins, P. In *Metal Nitrosyls*; Oxford University Press: New York, 1992. (j) Scheidt, W. R.; Ellison, M. K. *Acc. Chem. Res.* **1999**, *32*, 350. (k) Cooper, C. E. *Biochim. Biophys. Acta* **1999**, *1411*, 290. (l) Wieraszko, A.; Clarke, M. J.; Lang, D. R.; Lopes, L. G. F.; Franco, D. W. *Life Sci.* **2001**, *68*, 1535. (m) McCleverty, J. A. *Chem. Rev.* **2004**, *104*, 403. (n) Patra, A. K.; Mascharak, P. K. *Inorg. Chem.* **2003**, *42*, 7363. (o) Ghosh, K.; Eroy-Reveles, A. A.; Avila, B.; Holman, T. R.; Olmstead, M. M.; Mascharak, P. K. *Inorg. Chem.* **2004**, *43*, 2988. (p) Patra, A. K.; Rose, M. J.; Murphy, K. A.; Olmstead, M. M.; Mascharak, P. K. *Inorg. Chem.* **2004**, *43*, 4487. (q) Fricker, S. P.; Slade, E.; Powell, N. A.; Vaughn, O. J.; Henderson, G. R.; Murrer, S. A.; Megson, I. C.; Bisland, S. K.; Flitney, F. W. *Br. J. Pharmacol.* **1997**, *122*, 1441. (r) Bettache, N.; Carter, T.; Corrie, J. E. T.; Ogden, D.; Trentham, D. R. In *Methods in Enzymology*; Packer, L., Ed.; Academic Press: San Diego, CA, 1996; Vol. 268, p 266. (s) Davies, N.; Wilson, M. T.; Slade, E.; Fricker, S. P.; Murrer, B. A.; Powell, N. A.; Henderson, G. R. *J. Chem. Soc., Chem. Commun.* **1997**, 47. (t) Chen, Y.; Shepherd, R. E. *J. Inorg. Biochem.* **1997**, *68*, 183. (u) Slocik, J. M.; Ward, M. S.; Shepherd, R. E. *Inorg. Chim. Acta* **2001**, *317*, 290. (v) Lopes, L. G. F.; Wieraszko, A.; El-Sherif, Y.; Clarke, M. J. *Inorg. Chim. Acta* **2001**, *312*, 15. (w) Bezerra, C. W. B.; Silva, S. C.; Gambardella, M. T. P.; Santos, R. H. A.; Plicas, L. M. A.; Tfouni, E.; Franco, D. W. *Inorg. Chem.* **1999**, *38*, 5660. (x) Hui, J. W.-S.; Wong, W.-T. *Coord. Chem. Rev.* **1998**, *172*, 389. (y) Lee, S.-M.; Wong, W.-T. *Coord. Chem. Rev.* **1997**, *164*, 415.

(2) (a) Pandey, K. K. *Coord. Chem. Rev.* **1983**, *51*, 69. (b) Zang, V.; van Eldik, R. *Inorg. Chem.* **1990**, *29*, 4462. (c) Pham, E. K.; Chang, S. G. *Nature* **1994**, *369*, 139.

(3) Laverman, L. E.; Wanat, A.; Oszajca, J.; Stochel, G.; Ford, P. C.; van Eldik, R. *J. Am. Chem. Soc.* **2001**, *123*, 285.

(4) Wolak, M.; Stochel, G.; Zahl, A.; Schneppensieper, T.; van Eldik, R. *J. Am. Chem. Soc.* **2001**, *123*, 9780.

(5) (a) McCleverty, J. A. *Chem. Rev.* **1979**, *79*, 53. (b) Das, A.; Jones, C. J.; McCleverty, J. A. *Polyhedron* **1993**, *12*, 327. (c) Thiemens, M. H.; Trogler, W. C. *Science* **1991**, *251*, 932. (d) Feelisch, M., Stamler, J. S., Eds. *Methods in Nitric Oxide Research*; Wiley: Chichester, England, 1996. (e) Enemark, J. H.; Felthan, R. D. *Coord. Chem. Rev.* **1974**, *13*, 339.

(6) Mondal, B.; Paul, H.; Puranik, V. G.; Lahiri, G. K. *J. Chem. Soc., Dalton Trans.* **2001**, 481.

(7) Pipes, D. W.; Meyer, T. J. *Inorg. Chem.* **1984**, *23*, 2466.

(8) Chanda, N.; Mobin, S. M.; Puranik, V. G.; Datta, A.; Niemeyer, M.; Lahiri, G. K. *Inorg. Chem.* **2004**, *43*, 1056.

(9) Dovletoglou, A.; Adeyemi, S. A.; Meyer, T. J. *Inorg. Chem.* **1996**, *35*, 4120.

(10) Hadadzadeh, H.; DeRosa, M. C.; Yap, G. P. A.; Rezvani, A. R.; Crutchley, R. J. *Inorg. Chem.* **2002**, *41*, 6521.

(11) (a) Park, S. J.; Kim, D. H.; Kim, D. H.; Park, H. J.; Lee, D. N.; Kim, B. H.; Lee, W.-Y. *Anal. Sci.* **2001**, *17*, a93. (b) Nozaki, K.; Ikeda, N.; Ohno, T. *New J. Chem.* **1996**, *20*, 739. (c) Yi, H.; Crayston, J. A.; Irvine, J. T. S. *Dalton Trans.* **2003**, 685. (d) Slattery, S. J.; Gokaldas, N.; Mick, T.; Goldsby, K. A. *Inorg. Chem.* **1994**, *33*, 3621. (e) Haga, M.-A.; Tsunemitsu, A. *Inorg. Chim. Acta* **1989**, *164*, 137. (f) Uson, R.; Oro, L. A.; Ciriano, M. A.; Naval, M. M.; Apreda, M. C.; Foces-Foces, C.; Cano, F. H.; Garcia-Blanco, S. *J. Organomet. Chem.* **1983**, *256*, 331. (g) Panda, B. K.; Ghosh, K.; Chattopadhyay, S.; Chakravorty, A. *J. Organomet. Chem.* **2003**, *674*, 107. (h) Maji, M.; Sengupta, P.; Chattopadhyay, S. K.; Mostafa, G.; Schwalbe, C. H.; Ghosh, S. *J. Coord. Chem.* **2001**, *54*, 13. (i) Haga, M.-A.; Ali, Md. M.; Koseki, S.; Fujimoto, K.; Toshimura, A.; Nozaki, K.; Ohno, T.; Nakajima, K.; Stufkens, D. J. *Inorg. Chem.* **1996**, *35*, 3335.

(12) (a) Kim, B. H.; Lee, N.; Park, H. J.; Min, J. H.; Jun, Y. M.; Park, S. J.; Lee, W.-Y. *Talanta* **2004**, *62*, 595.

(13) (a) Mueller-Buschbaum, K.; Quitmann, C. C. *Inorg. Chem.* **2003**, *42*, 2742. (b) Chanda, N.; Sarkar, B.; Kar, S.; Fiedler, J.; Kaim, W.; Lahiri, G. K. *Inorg. Chem.* **2004**, *43*, 5128.

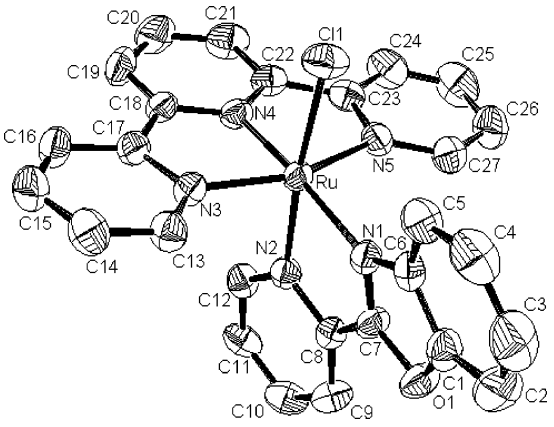

Figure 1. Structure of the cation of $[Ru(trpy)(L^1)Cl]ClO_4$ (**1**).

Though in principle the complexes can exist in the isomeric forms **A** and **B**, crystal structures of the representative complexes established that L^1-, L^3-, and L^4-derived species stabilize in form **A**, whereas form **B** was obtained preferentially in the complexes of L^2 (see later).

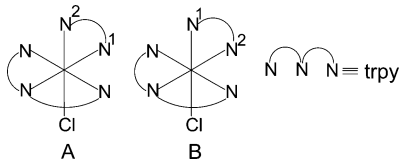

The nitrosyl complexes **13**−**15** were isolated as their perchlorate salts $\{[Ru^{II}(trpy)(L^{1,2,4})(NO)](ClO_4)_3\}$, but **15** was specifically isolated as a mixed perchlorate and nitrate salt $\{[Ru^{II}(trpy)(L^3)(NO)](ClO_4)_2(NO_3)\}$. The complexes gave satisfactory microanalytical data. The chloro (**1**−**4**), aqua (**5**−**8**), nitro (**9**−**12**), and nitrosyl (**13**−**16**) derivatives exhibited 1:1, 1:2, 1:1, and 1:3 conductivities, respectively. The electrospray mass spectral data authenticated the formation of the complexes in the solution state as well (see the Experimental Section).

Crystal structures of the representative complexes **1**, **2**, **13**, **15**, and **16** are shown in Figures1−5, and the structures of **4**, **9**, and **12** are placed in the Supporting Information (Figures S1−S3). Selected bond distances/angles and important crystallographic parameters are listed in Tables 1/2 and 3/4, respectively. The terpyridine ligand is coordinated to the ruthenium ion in the expected meridional fashion, with the ligand L being in the *cis* orientation.[8,14] The geometrical constraint arises due to the meridional mode of the trpy ligand, which has been reflected in their *trans* angles (Tables1 and 2). The central Ru−N(4) (trpy) bond length in the complexes is significantly shorter than the corresponding terminal Ru−N(3) and Ru−N(5) distances as observed on earlier occasions[6−8,10] (Tables 1 and 2).

The unsymmetrical azole-based ligands L^1−L^4 are bonded to the ruthenium ion via the azole (N^1) and the pyridyl (N^2) nitrogen donor centers, forming a five-membered neutral chelate ring. Out of the two possible geometrical isomers of [Ru(trpy)(L)(X)] (**A** and **B**), the isomeric form **A** (π-acceptor trpy and azole ring in the equatorial plane and the pyridine and chloride donors in the axial positions) has been stabilized in all the structures except **2**, where the isomer **B** (trpy and pyridine in the equatorial plane and the azole ring and chloride donors in the axial positions) has been selectively formed. As a consequence of isomeric structural forms, the Ru−N(4) (trpy) distance in **2** is ∼0.02 Å longer than that in **1** or **4**. This is attributed to the fact that Ru−N(4) in **2** is *trans* to the electron-withdrawing pyridyl ring nitrogen [N(2)] of L^2 as opposed to the azole ring nitrogen [N(1)] of L^1 or L^4 in **1** or **4**. Consequently, the Ru−N(2) distance in **2** is 0.05 Å longer than that in **1** or **4**, where the σ-donating and π-donating Cl^- is *trans* to Ru−N(2). Similarly, the *trans* configuration of the Cl^- group with respect to the azole ring in **2** makes the Ru−Cl bond distance slightly shorter at 2.397(3) Å relative to 2.402(12) or 2.4229(10) Å in **1** or **4**, respectively. The effect of isomeric structures has been nicely reflected in the Ru−N(1) (azole) distances, 2.092(3) and 2.066(6) Å in **1** and **2**, respectively. The *trans* angle involving N−Ru−Cl is ∼2.5° more tilted in **2** compared to **1** or **4** as a consequence of the small bite angle involving the five-membered azole ring.

The distances of Ru^{II}−N(1) (azole)/Ru^{II}−N(2) (pyridine) involving L^{1-4},[11g−i] Ru^{II}−N(3−5) involving trpy,[8,14] Ru^{II}−N(6) (NO_2),[6,8,15] and Ru^{II}−Cl[8,14] in the complexes (Tables 1 and 2) agree well with those in similar reported complexes.

The Ru^{II}−N(6) (NO_2) distance in **9** [2.029(3) Å] and **12** [2.035(3) Å] is comparable with that observed in the

Scheme 1

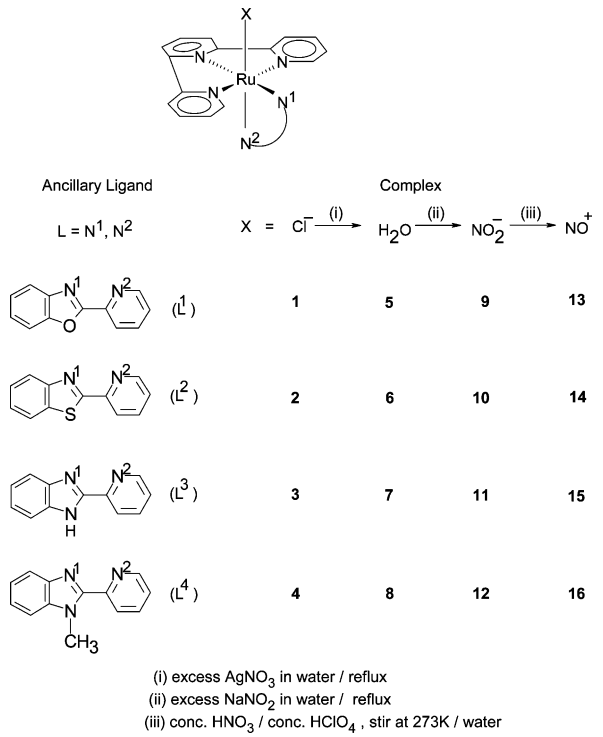

(14) (a) Mondal, B.; Chakraborty, S.; Munshi, P.; Walawalkar, M. G.; Lahiri, G. K. *J. Chem. Soc., Dalton Trans*. **2000**, 2327. (b) Catalano, V. J.; Heck, R. A.; Ohman, A.; Hill, M. G. *Polyhedron* **2000**, *19*, 1049. (c) Mondal, B.; Puranik, V. G.; Lahiri, G. K. *Inorg. Chem*. **2002**, 41, 5831. (d) Chanda, N.; Mondal, B.; Puranik, V. G.; Lahiri, G. K. *Polyhedron* **2002**, *21*, 2033.

(15) (a) Leising, R. A.; Kubow, S. A.; Churchill, M. R.; Buttrey, L. A.; Ziller, J. W.; Takeuchi, K. J. *Inorg. Chem*. **1990**, *29*, 1306. (b) Seddon, E. A.; Seddon, K. R. *The Chemistry of Ruthenium*; Elsevier: New York, 1984.

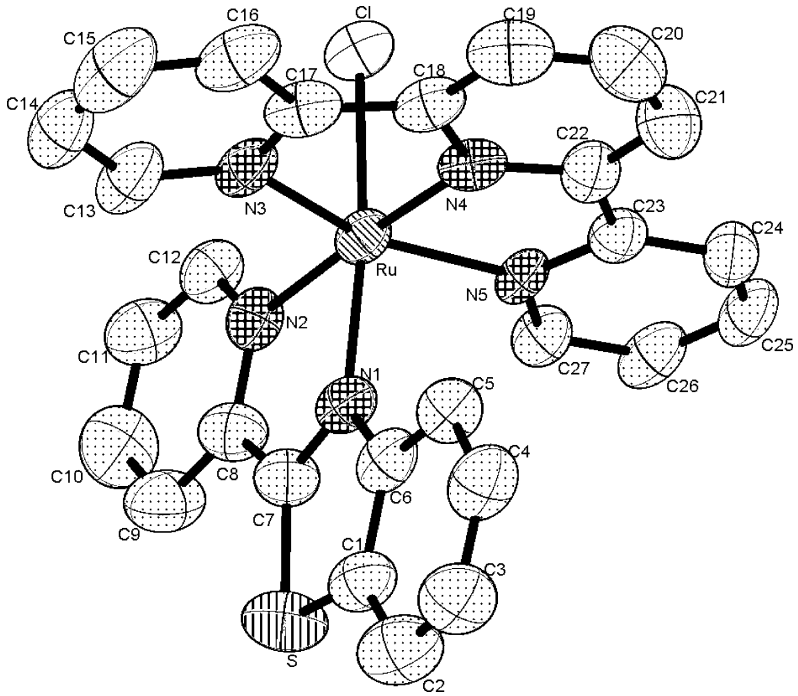

Figure 2. Structure of the cation of $[Ru(trpy)(L^2)Cl]ClO_4$ (**2**).

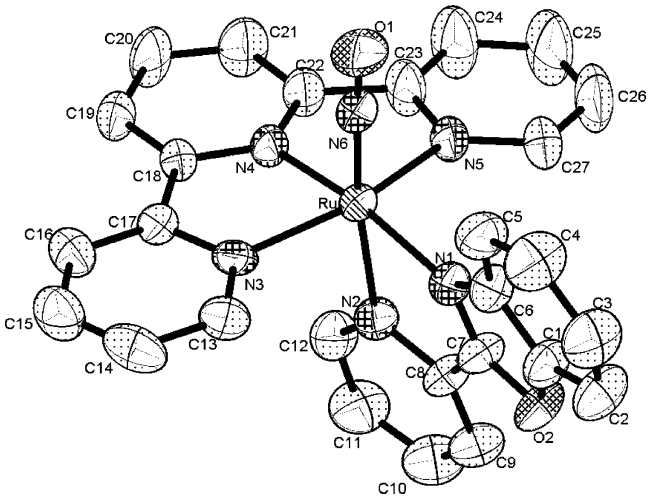

Figure 3. Structure of the cation of $[Ru(trpy)(L^1)(NO)](ClO_4)_3$ (**13**).

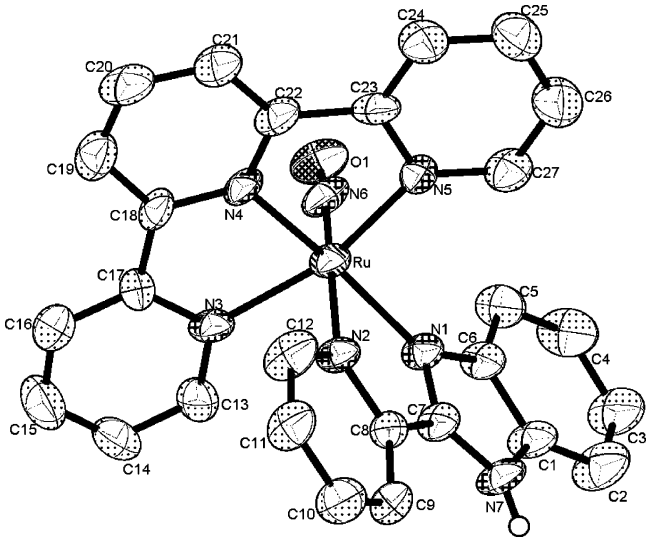

Figure 4. Structure of the cation of $[Ru(trpy)(L^3)(NO)](ClO_4)_2(NO_3)$ (**15**).

corresponding L = dpa complex [2.034(2) Å] but much shorter than that for the L = phenylazopyridine (pap) complex [2.057(6) Å]. The presence of strong $Ru^{II}-\pi^*(N{=}N)$ back-bonding *trans* to the NO_2 function enhances the Ru−NO_2 bond length.

As expected the $Ru^{II}-N(6)$ (NO) bond lengths, 1.749(5), 1.742(10), and 1.754(5) Å in **13**, **15**, and **16**, respectively, are significantly shorter than the single-bonded Ru−NO_2 distances [**9**, 2.029(3) Å; **12**, 2.035(3) Å]. Ru−NO bonds in the present set of complexes are slightly shorter (0.011−0.023 Å) than that reported for $[Ru(trpy)(dpa)(NO)](ClO_4)_3$ [1.765(12) Å].[8] However, these are ∼0.08 Å shorter than that in $[Ru(trpy)(pp)(NO)](PF_6)_2$.[10] This is attributed to the *trans* orientation of the Ru−NO group with respect to the electron-withdrawing pyridine ring of L in **13**, **15**, **16**, and dpa complexes as opposed to the strongly σ-donating carbanion center in the cyclometalated arrangement in the pp complex. This effect has also been reflected in their ν(NO) frequencies and redox potentials (see later). The triple bond feature of the N−O bond length, N(6)−O(1), 1.130(6), 1.130(10), and 1.129(5) Å, in conjunction with the close to linear mode of Ru−NO, Ru−N(6)−O(1), 177.4(5)°, 174.4(9)°, and 176.9(4)° in **13**, **15**, and **16**, respectively, revealed the π-acceptor characteristics of the coordinated NO^+ ligand in the complexes.[6−10] The Ru−N−O bond angle in the dpa complex is 176.2(12)°; however, the same angle in the pp complex is in a semibent mode, 167.1(4)°. The presence of a σ-donating phenyl ligand (carbanion center) *trans* to the nitrosyl function in the pp complex decreases its electrophilicity to a large extent, leading to a slightly bent metal−nitrosyl bond.

Nitrosyl complexes **13**−**16** exhibited a wide variation of ν(NO) stretching frequency (1957−1932 cm^{-1}) [Table 5 and

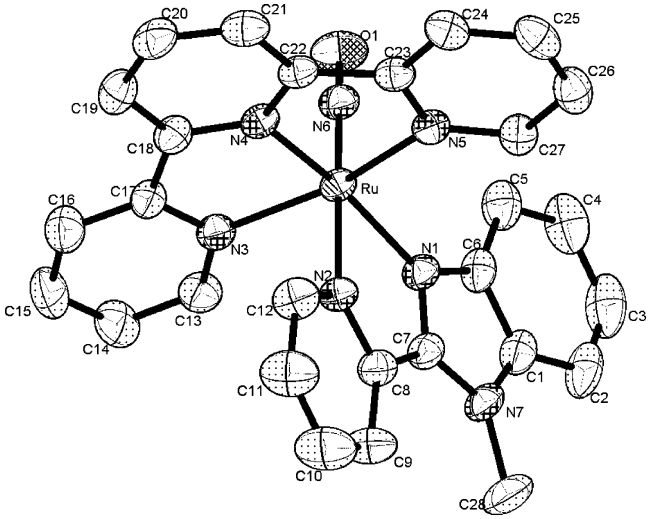

Figure 5. Structure of the cation of $[Ru(trpy)(L^4)(NO)](ClO_4)_3$ (**16**).

Table 1. Selected Bond Distances (Å) and Angles (deg) for **1**, **2**, and **4**

bond length/ bond angle	**1**	**2**	**4**
Ru−N(1)	2.092(3)	2.066(6)	2.099(3)
Ru−N(2)	2.058(3)	2.108(6)	2.060(3)
Ru−N(3)	2.058(4)	2.082(6)	2.066(3)
Ru−N(4)	1.939(3)	1.953(6)	1.945(3)
Ru−N(5)	2.077(4)	2.057(5)	2.058(3)
Ru−Cl(1)	2.402(12)	2.394(2)	2.4229(10)
N(1)−Ru−Cl(1)	96.06(10)	171.1(2)	96.92(9)
N(2)−Ru−Cl(1)	173.64(10)	93.56(19)	173.38(9)
N(3)−Ru−Cl(1)	89.31(10)	88.48(17)	91.21(9)
N(4)−Ru−Cl(1)	89.86(11)	87.03(18)	87.49(9)
N(5)−Ru−Cl(1)	89.95(10)	90.40(17)	88.89(9)
N(5)−Ru−N(1)	100.46(14)	92.1(2)	96.45(12)
N(1)−Ru−N(2)	77.77(13)	77.6(3)	77.74(12)
N(2)−Ru−N(3)	93.24(14)	105.1(3)	86.32(12)
N(3)−Ru−N(4)	80.02(14)	78.7(3)	79.64(12)
N(4)−Ru−N(5)	79.70(15)	79.5(3)	80.08(12)
N(3)−Ru−N(1)	99.79(13)	92.3(2)	103.69(12)
N(4)−Ru−N(1)	174.08(14)	101.8(3)	174.37(12)
N(3)−Ru−N(5)	159.71(14)	158.2(3)	159.69(12)
N(2)−Ru−N(5)	89.67(14)	96.7(2)	95.55(12)
N(4)−Ru−N(2)	96.32(14)	176.2(2)	98.09(12)

Supporting Information (Figure S4)]. The 2-(2-pyridyl)-oxazole-derived complex **13** showed the maximum ν(NO) frequency at 1957 cm^{-1}. However, the ν(NO) frequency of the analogous 2-(2-pyridyl)benzthiazole-based complex **14** appeared at a much lower value of 1941 cm^{-1}, which happened to be almost identical to that of the 2-(2-pyridyl)-benzimidazole complex **15** (1940 cm^{-1}). The introduction of an electron-donating Me group in the benzimidazole fragment of L^4 in **16**, however, reduced the frequency reasonably to 1932 cm^{-1}. The lowering of the ν(NO) stretching frequency on switching from **13** (1957 cm^{-1}) to **15** (1940 cm^{-1}) to **16** (1932 cm^{-1}) is understandable as the ligand field strength is in the order $L^1 > L^3 > L^4$ (see later). The same argument cannot be straightaway extended to **14** as unlike L^3 and L^4 in **15** and **16**, respectively, the geometrical configurations of L^2 and L^1 in **14** and **13**, respectively, are altogether different (isomers **B** and **A**, respectively). The preferential *trans* orientation of the electron-withdrawing pyridyl ring with respect to the NO function in **13** makes it more electrophilic compared to **14**, in which the azole ring is *trans* to NO. Moreover, the ligand

Table 2. Selected Bond Distances (Å) and Angles (deg) for **9**, **12**, **13**, **15**, and **16**

bond length/ bond angle	**9**	**12**	**13**	**15**	**16**
Ru−N(1)	2.101(3)	2.101(3)	2.083(4)	2.053(7)	2.078(4)
Ru−N(2)	2.101(3)	2.092(3)	2.115(4)	2.112(8)	2.103(4)
Ru−N(3)	2.077(3)	2.084(3)	2.075(5)	2.053(8)	2.085(4)
Ru−N(4)	1.956(3)	1.959(3)	1.982(4)	1.989(7)	1.991(4)
Ru−N(5)	2.056(3)	2.064(3)	2.080(4)	2.066(8)	2.072(4)
Ru−N(6)	2.029(3)	2.035(3)	1.749(5)	1.742(10)	1.754(5)
N(6)−O(1)	1.193(5)	1.247(4)	1.130(6)	1.130(10)	1.129(5)
N(6)−O(2)	1.225(5)	1.252(4)			
N(1)−Ru−N(6)	96.87(13)	98.19(11)	95.8(2)	95.4(4)	97.42(18)
N(2)−Ru−N(6)	174.02(13)	175.23(11)	172.4(2)	171.3(3)	173.62(17)
N(3)−Ru−N(6)	89.68(14)	90.79(12)	94.1(2)	92.3(4)	93.13(18)
N(4)−Ru−N(6)	89.34(13)	85.94(12)	95.2(2)	96.5(4)	95.50(18)
N(5)−Ru−N(6)	89.67(14)	90.58(12)	94.4(2)	94.4(4)	95.78(18)
N(5)−Ru−N(1)	99.83(12)	100.67(11)	100.04(18)	98.3(3)	97.89(16)
N(1)−Ru−N(2)	77.42(12)	77.18(11)	77.02(17)	77.6(3)	77.20(16)
N(2)−Ru−N(3)	89.65(12)	88.91(11)	89.72(17)	84.0(3)	84.58(16)
N(3)−Ru−N(4)	79.76(13)	79.32(12)	79.33(17)	79.6(3)	79.58(17)
N(4)−Ru−N(5)	79.90(13)	79.60(12)	79.94(17)	80.0(4)	79.85(16)
N(3)−Ru−N(1)	100.44(13)	100.14(11)	99.03(17)	100.8(3)	100.57(16)
N(4)−Ru−N(1)	173.78(13)	175.85(11)	168.96(19)	168.0(3)	167.05(16)
N(3)−Ru−N(5)	159.65(13)	158.73(11)	158.23(18)	159.0(3)	158.26(17)
N(2)−Ru−N(5)	93.02(13)	91.42(11)	84.45(19)	91.7(3)	88.42(16)
N(4)−Ru−N(2)	96.38(12)	98.68(11)	92.03(19)	90.5(3)	89.96(16)
Ru−N(6)−O(1)	120.8(3)	121.7(2)	177.4(5)	174.4(9)	176.9(4)
Ru−N(6)−O(2)	122.1(3)	120.6(3)			
O(1)−N(6)−O(2)	117.1(4)	117.6(3)			

field strength of L^2 was also found to be less than that of L^1 in rhenium complexes $[Re(L^1)/(L^2)(Cl)_3(O)]$ and $[Re(L^1)/(L^2)(Cl)_3(NPh)]$.[16]

The ν_{NO} stretching frequency of **13**−**16** is much higher than that in the reported analogous {Ru(trpy)(NO)(L)} complexes, where L = σ-donating pp (1858 cm^{-1})[10] and acac (1914 cm^{-1}).[9] The ν_{NO} value of **13** is lower than that for L = strongly π-acidic pap (1960 cm^{-1})[6] but greater than that for the bpy (1952 cm^{-1})[7] and dpa (1945 cm^{-1})[8] derivatives. On the other hand, the ν_{NO} values for **14**/**15** and **16**, respectively, are slightly and reasonably less in comparison to that of the dpa complex.

Crystal structures of the analogous Ru−trpy-derived nitrosyl complexes $[Ru^{II}(trpy)(L)(NO)]^{3+}$ with L = pap, bpy, and acac are currently unknown. However, the correlation between the structural (Ru−NO distance and Ru−N−O angle) and the ν_{NO} data for **13**, **15**, **16**, Ru−dpa, and Ru−pp complexes is valuable in understanding the role of ancillary ligands (L) toward the extent of electrophilicity of the coordinated nitrosyl function in such complexes.

^{1}H NMR spectra of the chloro derivatives **1**−**4** in $(CD_3)_2$-SO are shown in the Supporting Information (Figure S5) (the data are listed in the Experimental Section). They exhibited a calculated number (19) of partially overlapping aromatic signals in each case in the range δ = 9.2−7.0 ppm, 11 from the terpyridine ligand and 8 from the azole-based ancillary ligands L^1−L^4. The observed distinct 19 signals implied the presence of one particular isomer (**A** or **B**) in the solution state as well. The NH proton of the benzimidazole derivative **3** appeared at 14.6 ppm, and it disappeared on exchange with D_2O, which supports the preferential binding via the neutral N^1 donor center of the benzimidazole group as stated above. The signal of the NMe group of **4** appeared at 4.53 ppm.

(16) Gangopadhyay, J.; Sengupta, S.; Bhattacharyya, S.; Chakraborty, I.; Chakravorty, A. *Inorg. Chem.* **2002**, *41*, 2616.

Table 3. Crystallographic Data for **1**, **2**, **4**, and **9**

empirical formula	$C_{27}H_{19}Cl_2N_5O_5Ru$ (**1**)	$C_{54.5}H_{40}Cl_4N_{10}O_{8.5}Ru_2S_2$ (**2**)	$C_{28}H_{22}Cl_2N_6O_4Ru$ (**4**)	$C_{27}H_{20}Cl_1N_6O_{7.5}Ru$ (**9**)
fw	665.44	1379.02	678.49	685.01
radiation	Mo Kα	Mo Kα	Mo Kα	Mo Kα
cryst symmetry	orthorhombic	triclinic	monoclinic	orthorhombic
space group	*Pcab*	$P\bar{1}$	$P2_1/n$	*Pbca*
a (Å)	11.191(1)	13.606(2)	14.398(1)	11.196(1)
b (Å)	14.194(1)	15.253(2)	12.162(1)	14.423(1)
c (Å)	33.151(1)	15.602(2)	15.477(1)	34.039(6)
α (deg)	90.0	113.505(2)	90.0	90.0
β (deg)	90.0	93.348(2)	92.644(6)	90.0
γ (deg)	90.0	105.418(2)	90.0	90.0
V (Å^3)	5265.9(7)	2812.3(6)	2707.3(4)	5498.5(12)
Z	8	2	4	8
μ (mm^{-1})	0.848	0.866	0.824	0.728
T (K)	293(2)	293(2)	293(2)	293(2)
D_{calcd} (g cm^{-3})	1.679	1.628	1.665	1.655
2*θ* range (deg)	2.46−49.86	2.90−50.00	3.78−49.88	2.38−49.82
no. of unique data	3762	9875	4396	4227
R1 ($I > 2\sigma(I)$)	0.0347	0.0715	0.0339	0.0357
wR2 (all data)	0.0896	0.2138	0.0934	0.0918
GOF	1.055	1.032	1.080	1.063

Table 4. Crystallographic Data for **12**, **13**, **15**, and **16**

empirical formula	$C_{28}H_{22}Cl_1N_7O_6Ru$ (**12**)	$C_{57}H_{42.5}Cl_6N_{13.5}O_{28}Ru_2$ (**13**)	$C_{30}H_{25}Cl_2N_8O_{13}Ru$ (**15**)	$C_{28}H_{26}Cl_3N_7O_{15}Ru$ (**16**)
fw	689.05	1779.39	877.55	907.98
radiation	Mo Kα	Mo Kα	Mo Kα	Mo Kα
cryst symmetry	monoclinic	monoclinic	monoclinic	trjclinic
space group	*P*21/*a*	Cc	*C*2/*c*	*P*1
a (Å)	13.702(1)	21.171(2)	39.07(3)	9.283(1)
b (Å)	13.805(1)	30.040(3)	9.625(8)	10.432(2)
c (Å)	15.196(1)	14.837(1)	19.353(16)	18.729(3)
α (deg)	90.0	90.0	90.0	104.955(2)
β (deg)	101.520(6)	133.379(1)	111.644(13)	92.655(2)
γ (deg)	90.0	90.0	90.0	95.718(2)
V (Å^3)	2816.5(4)	6858.3(11)	6765.0(9)	1738.6(5)
Z	4	4	8	2
μ (mm^{-1})	0.708	0.770	0.702	0.763
T (K)	293(2)	293(2)	293(2)	293(2)
D_{calcd} (g cm^{-3})	1.625	1.723	1.721	1.734
2*θ* range (deg)	2.72−49.92	2.72−50.00	4.24−47.00	4.06−50.00
no. of unique data	4345	11986	5014	6093
R1 ($I > 2\sigma(I)$)	0.0330	0.0409	0.0744	0.0544
wR2 (all data)	0.0817	0.1136	0.1846	0.1428
GOF	1.065	0.997	0.992	1.063

It may be noted that the spin−spin coupling constant in the case of complex **2**, possessing the isomeric structure **B**, is much lower (J/Hz = 3.5−5.7) than those of complexes **1**, **3**, and **4** (J/Hz = 6−9), existing in the isomeric form **A**.

The NMR spectra of the nitro (**9**−**12**) and nitrosyl (**13**−**16**) complexes in $(CD_3)_2SO$ are very similar to those of the corresponding chloro derivatives except slight changes in the position and profile of the signals based on the sixth ligand (Cl^-, NO_2^- or NO^+), indicating the stereoretentive transformation processes.

Chloro complexes **1**−**4** exhibited a reversible $Ru^{III}-Ru^{II}$ couple in the range of 0.59−0.76 V versus SCE in CH_3CN (Table 5, Figure 6), and the stability of the Ru^{II} state follows the order **1** ≈ **2** > **3** > **4**. However, the oxidation potentials of the rhenium−L^1 based complexes $[Re(L^1)(Cl)_3(O)]/[Re(L^1)(Cl)_3(NPh)]$ were found to be higher than those of thiazole (L^2) analogues $[Re(L^2)(Cl)_3(O)]/[Re(L^2)(Cl)_3(NPh)]$.[16] Thus, it may be reasonable to assume that the observed similar redox stability of the Ru^{II} state in **1** and **2** originated primarily on the basis of their isomeric geometries. On replacement of the chloro function by the stronger electron-withdrawing NO_2^- group in **9**−**12**, the stability of the Ru^{II} state expectedly increased further by ∼200 mV in each case (0.80−0.95 V) (Table 5).[8] The ruthenium(II) state in **1**−**4** as well as in **9**−**12** is reasonably less stable than that of the corresponding analogous complexes incorporating L = *π*-acidic pap (Cl^-, 1.07 V; NO_2^-, 1.39 V),[6] bpy (Cl^-, 0.81 V; NO_2^-, 1.05 V),[7] 3,6-di(pyrid-2-yl)pyridazine (Cl^-, 0.89 V),[17] bipyrazine (Cl^-, 1.07 V),[18] and *cis*-1,2-bis(diphenylphosphino)ethylene (Cl^-, 1.23 V),[9] but more stable in comparison to that of complexes incorporating L = *σ*-donating acac (Cl^-, 0.26 V; NO_2^-, 0.42 V)[9] or pp (Cl^-, 0.21 V).[10] However, in relation to the L = dpa (Cl^-, 0.64 V; NO_2^-, 0.88 V)[8] complexes, the present set of complexes (**1**−**4** and **9**−**12**) can be classified into two distinct groups in terms of the ligand field strength of the ancillary ligands (L), and it follows the order $L^1 \approx L^2 >$ dpa $> L^3 \approx$ L.[4]

The expected terpyridine-based successive two reductions appeared in the range of −1.26 to −1.80 V versus SCE (Table 5).[6−8,18]

In addition to the terpyridine-based reductions, nitrosyl complexes **13**−**16** also systematically displayed two more successive reductions at a much higher potential, ranges of 0.49 → 0.31 V and −0.21 → −0.37 V (Table 5, Figure 6),

(17) Catalano, V. J.; Heck, R. A.; Immoos, C. E.; Ohman, A.; Hill, M. G. *Inorg. Chem.* **1998**, *37*, 2150.
(18) Gerli, A.; Reedijk, J.; Lakin, M. T.; Spek, A. L. *Inorg. Chem.* **1995**, *34*, 1836.

Table 5. Electrochemical[a] and EPR[b] Data

compd		E^o_{298}/V (ΔE_p/mV)[a]			ν(NO)/ cm^{-1} [c]	$g_1 = g_2$	g_3	$\langle g \rangle$	A/G
		$Ru^{III}-Ru^{II}$ couple	ligand reduction						
			nitrosyl	trpy					
L^1	**1**	0.75 (90)		−1.38 (90)					
				−1.62 (180)					
	9	0.95 (120)		−1.37 (70)					
				−1.65 (100)					
	13		0.45 (100)	−1.41 (50)	1957	2.013	1.888	1.972	28
			−0.24 (100)	−1.70 (90)					
L^2	**2**	0.76 (90)		−1.32 (70)					
				−1.58 (180)					
	10	0.95 (130)		−1.32 (90)					
				−1.66 (88)					
	14		0.49 (100)	−1.261 (55)	1941	2.016	1.889	1.975	27
			−0.21 (110)	−1.437 (100)					
L^3	**3**	0.61(90)		−1.54 (80)					
				−1.69 (82)					
	11	0.83 (140)		−1.54 (60)					
				−1.63 (75)					
	15		0.33 (100)	−1.55 (45)	1940	2.013	1.885	1.971	24
			−0.37 (130)	−1.68 (64)					
L^4	**4**	0.59 (100)		−1.50 (100)					
				−1.63(150)					
	12	0.80 (120)		−1.50 (80)					
				−1.75 (140)					
	16		0.31 (90)	−1.60 (100)	1932	2.013	1.878	1.969	27
			−0.36 (130)	−1.80 (150)					

[a] In CH_3CN versus SCE. [b] In CH_3CN at 77 K. [c] In KBr disk.

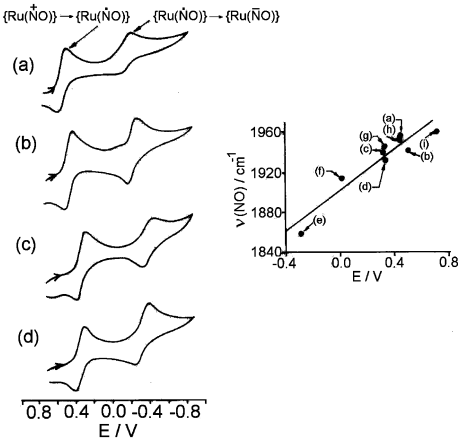

Figure 6. Cyclic voltammograms of (a) $[Ru^{II}(trpy)(L^1)(NO)](ClO_4)_3$ (**13**), (b) $[Ru^{II}(trpy)(L^2)(NO)](ClO_4)_3$ (**14**), (c) $[Ru^{II}(trpy)(L^3)(NO)](ClO_4)_2(NO_3)$ (**15**), and (d) $[Ru^{II}(trpy)(L^4)(NO)](ClO_4)_3$ (**16**) in CH_3CN. The inset shows a plot of the potential of the $\{Ru(NO^+)\} \rightarrow \{Ru(NO^\bullet)\}$ couple versus the ν(NO) of nine related complexes as stated in the text: (a−d), (e) pp, (f) acac, (g) dpa, (h) bpy, (i) pap.

which are assigned as the reductions associated with the coordinated nitrosyl function, $[Ru^{II}(trpy)(L^{1-4})(NO^+)]^{3+} \rightarrow [Ru^{II}(trpy)(L^{1-4})(NO^\bullet)]^{2+}$ and $[Ru^{II}(trpy)(L^{1-4})(NO^\bullet)]^{2+} \rightarrow [Ru^{II}(trpy)(L^{1-4})(NO^-)]^+$, respectively.[6−10] The first step ($Ru-NO^+ \rightarrow Ru-NO^\bullet$) reduction potentials follow the order **14** > **13** ≫ **15** = **16** (Table 5).

The $Ru^{II}-NO \rightarrow Ru^{II}-NO^\bullet$ reduction potential for the analogous complexes with L = pap,[6] bpy,[7] dpa,[8] acac,[9] and pp[10] appeared at 0.72, 0.45, 0.34, 0.02, and −0.275 V, respectively. A close look at their reduction potentials and the corresponding ν(NO) values (1960, 1952, 1945, 1914, and 1858 cm^{-1}, respectively) revealed that the potential decreases with a decrease in ν(NO). However, the earlier observed general relation between $E°(Ru^{II}-NO^+/Ru^{II}-NO^\bullet)$ and ν(NO) does not hold true, particularly for **13** and **14** (Table 5). The different *isomeric structural forms* in **13** and **14** (as stated above) can be considered as the most likely dominating factor toward the observed apparent mismatch between the ν(NO) values and the reduction potential data.

Consequently, the plot of $E_{1/2}$ of the $Ru-NO^+/Ru-NO^\bullet$ couple versus ν(NO) for the known nine {(trpy)Ru(L)(NO)} derivatives, where L corresponds to ancillary ligands with different electronic natures (pap, **13**, bpy, dpa, **14**, **15**, **16**, acac, pp) yielded an overall linear relationship (Figure 6, inset).[8,10] Although the first-step-reduced species $Ru-NO^\bullet$ was reasonably stable on the coulometric time scale at 298 K, the second-step process, $Ru-NO^\bullet \rightarrow Ru-NO^-$ was found to be unstable even at 273 K.

Coulometrically generated one-electron-reduced species $\mathbf{13}^- - \mathbf{16}^-$ in CH_3CN [n = 1.07, 1.09, 0.96, and 1.11 for **13**, **14**, **15**, and **16**, respectively, where $n = Q/Q'$ (Q' is the calculated Coulomb count for one-electron transfer, and Q is the Coulomb count found after exhaustive electrolysis)] displayed nearly axial type EPR spectra at 77 K with nitrogen hyperfine splittings (average hyperfine splitting $A \approx 26$ G) (Figure 7, Table 5). The average $\langle g \rangle$ factor derived from $\langle g \rangle = [^1/_3(g_1^2 + g_2^2 + g_3^2)]^{1/2}$ (Table 5) is close to the free radical value (∼2.0), which signifies that the reduction process is largely centered around the nitrosyl function as assigned above.[8,19] It may be noted that the earlier reported nitrosyl ($NO^\bullet$) complexes *trans*-$[Ru^{II}(H_2O)(cyclam)(NO^\bullet)]^+$ and *trans*-$[Ru^{II}(H_2O)(NH_3)_4(NO^\bullet)]^+$ also displayed similar nearly axial

(19) (a) de Souza, V. R.; da Costa Ferreira, A. M.; Toma, H. E. *Dalton Trans*. **2003**, 458. (b) McGarvey, B. R.; Ferro, A. A.; Tfouni, E.; Bezerra, C. W. D.; Bagatin, I. A.; Franco, D. W. *Inorg. Chem*. **2000**, *39*, 3577. (c) Callahan, R. W.; Meyer, T. J. *Inorg. Chem*. **1977**, *16*, 574. (d) Diversi, P.; Fontani, M.; Fuligni, M.; Laschi, F.; Marchetti, F.; Matteoni, S.; Pinzino, C.; Zanello, P. *J. Organomet. Chem*. **2003**, *675*, 21.

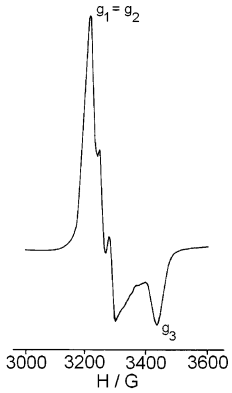

Figure 7. EPR spectrum of electrogenerated $[Ru^{II}(trpy)(L^2)(NO^{\bullet})]^{2+}$ (**14**$^-$) in CH_3CN at 77 K.

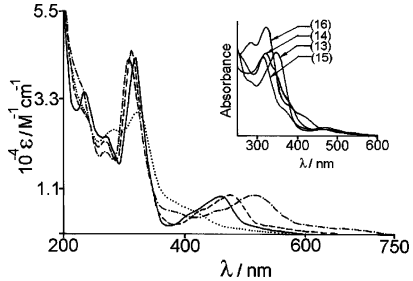

Figure 8. Electronic spectra in acetonitrile of $[Ru^{II}(trpy)(L^4)(Cl)]ClO_4$ (**4**) (-·-·-), $[Ru^{II}(trpy)(L^4)(H_2O)](ClO_4)_2$ (**8**) (—), $[Ru^{II}(trpy)(L^4)(NO_2)]ClO_4$ (**12**) (---), and $[Ru^{II}(trpy)(L^4)(NO)](ClO_4)_3$ (**16**) (···). The inset shows the spectra of the nitrosyl derivatives **13**−**16** in the range 600−250 nm.

EPR spectra ($g_x = g_y \approx 2.0$ and $g_z \approx 1.9$) with nitrogen hyperfine splittings at 77 K, where the correspondence of the EPR spectrum with the $Ru^{II}-NO^{\bullet}$ radical species was specifically established via the theoretical studies.[19b]

Ru^{II}-based MLCT [$Ru^{II} \rightarrow \pi^*$(trpy), 524−365 nm] and intraligand transitions were observed in the visible and UV regions, respectively (see the Experimental Section) (Figure 8).[6−8,18] On the basis of the relative stabilization of the Ru^{II} state, the energy of the $Ru^{II} \rightarrow$ trpy based MLCT band follows the order: $Cl^- < NO_2^- < H_2O \ll NO^+$ for a particular L.[20] However, the MLCT band position for a particular X (X = Cl, H_2O, NO_2, or NO) varies slightly depending on the ancillary ligands (L) (see the Experimental Section). The differences in energy between the MLCT transitions of the nitroso $[Ru(trpy)(L^{1-4})(NO)]^{3+}$ and the corresponding nitro $[Ru(trpy)(L^{1-4})(NO_2)]^+$ derivatives have been calculated to be 114, 100, 115, and 76 nm for L = L^1, L^2, L^3, and L,[4] respectively. The differences in energy for L = pap,[6] bpy,[7] and dpa[8] were reported to be ∼150, ∼130, and 30 nm, respectively.

The luminescence properties of the chloro (**1**−**4**), nitro (**9**−**12**), and aqua (**5**−**8**) derivatives were checked in EtOH−MeOH (4:1) and dichloromethane, respectively. Excitation of the complexes on the MLCT band near 500 nm caused a very weak emission at 298 K. However, in the glassy medium (77 K) they exhibited reasonably strong emissions near 700 nm (Figure 9, Table 6) with a quantum yield (ϕ) in the range of 0.06−0.27, reference to $Ru(bpy)_3^{2+}$ (ϕ = 0.34).[21] For a particular L the value of ϕ follows the order $NO_2^- > H_2O > Cl^-$. Since the emission quantum yield is primarily controlled by the σ-donor strength of the ligand moiety, it may therefore be inferred that the azole-based ancillary ligands L^1-L^4 in the complexes have a weaker ligand field strength than bpy. A similar effect has also been observed in their metal redox potentials described earlier (Table 5). The emission of ruthenium(II) polypyridyl complexes is known to originate from the triplet MLCT state,[22] and so, it is formally a phosphorescence process.

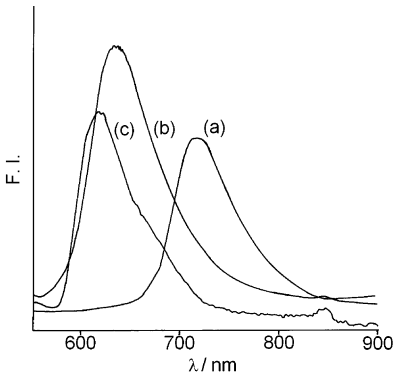

Figure 9. Emission spectra of (a) $[Ru^{II}(trpy)(L^1)(Cl)]ClO_4$ (**1**), (b) $[Ru^{II}(trpy)(L^1)(NO_2)]ClO_4$ (**9**) in 4:1 EtOH−MeOH, and (c) $[Ru^{II}(trpy)(L^1)(H_2O)](ClO_4)_2$ (**5**) in CH_2Cl_2 at 77 K.

Table 6. Emission Data[a]

complex		λ_{max} excitation	λ_{max} emission	quantum yield/ϕ
L^1	**1**	516	712	9.73×10^{-2}
	5	458	607	1.09×10^{-1}
	9	472	634	2.01×10^{-1}
L^2	**2**	525	727	6.76×10^{-2}
	6	470	608	1.51×10^{-1}
	10	480	638	2.73×10^{-1}
L^3	**3**	510	719	5.76×10^{-2}
	7	458	610	1.38×10^{-1}
	11	474	643	2.01×10^{-1}
L^4	**4**	517	723	6.90×10^{-2}
	8	462	607	1.42×10^{-1}
	12	472	641	2.36×10^{-1}

[a] Emission data in EtOH−MeOH (4:1) for chloro and nitro derivatives and in CH_2Cl_2 for the aqua complexes at 77 K.

Conversion of $[Ru^{II}(trpy)(L^{1-4})(NO)]^{3+}$ (13−16) → $[Ru^{II}(trpy)(L^{1-4})(NO_2)]^+$ (9−12). The nitrosyl complexes **13**−**16** are stable in the solid state; however, in aqueous medium they only slowly transformed into the corresponding nitro derivative. The rate of conversion of nitroso (**13**−**16**) to nitro (**9**−**12**) complexes $\{[Ru^{II}(trpy)(L^{1-4})(NO)]^{3+} + H_2O \rightarrow [Ru^{II}(trpy)(L^{1-4})(NO_2)]^+ + 2H^+\}$ was monitored spectrophotometrically at three different temperatures in water. The well-defined isobestic points (Figure 10) suggest the presence of nitrosyl and nitro species in appreciable concentrations during the conversion process. The pseudo-first-

(20) Mondal, B.; Walawalkar, M. G.; Lahiri, G. K. *J. Chem. Soc., Dalton Trans.* **2000**, 4209.

(21) (a) Alsfasser, R.; van Eldik, R. *Inorg. Chem.* **1996**, *35*, 628. (b) Chen, P.; Duesing, R.; Graff, D. K.; Meyer, T. J. *J. Phys. Chem.* **1991**, *95*, 5850.

(22) (a) Sarkar, B.; Laye, R. H.; Mondal, B.; Chakraborty, S.; Paul, R. L.; Jeffery, J. C.; Puranik, V. G.; Ward, M. D.; Lahiri, G. K. *J. Chem. Soc., Dalton Trans.* **2002**, 2097. (b) Juris, A.; Balzani, V.; Barigelletti, F.; Campagna, S.; Belser, P.; Von Zelewsky, A. *Coord. Chem. Rev.* **1988**, *84*, 85.

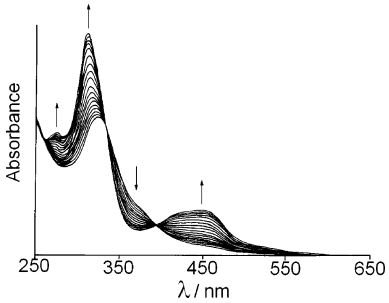

Figure 10. Time evolution of the electronic spectra of a changing solution of $[Ru^{II}(trpy)(L^4)(NO^+)]^{3+} \rightarrow [Ru^{II}(trpy)(L^4)(NO_2)]^+$ in water at 303 K. The arrows indicate an increase or decrease in band intensities as the reaction proceeds.

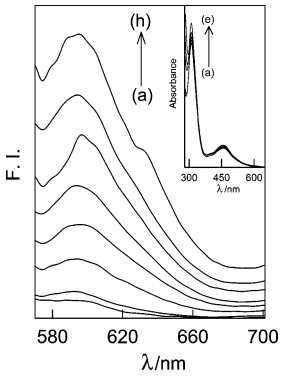

Figure 11. (a) Emission spectra of 70 μM **7** in TBS at 298 K without DNA. (b−h) Emission spectra of 10, 20, 30, 40, 50, 60, and 70 μM **7** in TBS, respectively, at 298 K, in the presence of 50 μM CT DNA (λ_{ex} = 454 nm in all cases). The inset shows the UV−vis spectra of 50 μM **7** in the presence of (a) 0, (b) 25, (c) 40, (d) 175, and (e) 275 μM CT DNA in TBS.

order rate constants (k), activation parameters ($\Delta H^{\ddagger}/\Delta S^{\ddagger}$), and equilibrium constants (K) are listed in Table 7. The rate constant values justify the slow conversion process, and in the case of **15** virtually no conversion was noticed in the temperature range 303−313 K. Therefore, the transformation for **15** was monitored specifically in a higher temperature range, 323−343 K, and the overall order appears to be **13** > **14** > **16** ≫ **15**. However, simply on the basis of the ν(NO) data, the order of the rate constant is expected to be **13** ≫ **14** ≈ **15** > **16** as the reactivity of the coordinated NO^+ toward the nucleophile is known to be a function of its extent of electrophilicity.

The low equilibrium constant values (0.4−3.8) in combination with the slow-rate processes (Table 7) revealed that for the present set of complexes the conversion of nitrosyl to nitro is not a favorable process both from the thermodynamic and kinetic points of views, although the NO^+ functions in **13** and **14**−**16** can be considered as strongly and moderately electrophilic centers, respectively, particularly on the basis of their ν(NO) frequencies (1957 and 1941−1932 cm^{-1}) and reduction potential data [$E_{1/2}(NO^+ \rightarrow NO^{\bullet})$ = 0.51→ 0.33 V]. It may be noted that for the bpy[7] and pap[6] complexes the equilibrium constant values of the Ru−NO^+ → Ru−NO_2 process are substantially high [10^{23} (in alkaline medium) and 10^5 (in dry acetonitrile and in the presence of a controlled concentration of water, 50 times excess with respect to the complex), respectively], as is also expected from their high ν(NO) frequencies (1953 and 1960 cm^{-1}, respectively).[6,7] Thus, the observed unusual stability of the nitrosyl complexes **13**−**16**, in general, and more surprisingly the stability of the benzoxazole derivative **13** even in the aqueous solution, for which the ν(NO) value (1957 cm^{-1}) is rather higher than that of the bpy analogue, are not clear at present. Further studies with newer examples will therefore be useful in establishing the correlation among the structure, ν(NO) frequency, reduction potential, and stability of the nitrosyl species.

The magnitude and sign of $\Delta H^{\ddagger}$ and $\Delta S^{\ddagger}$ follow the same trend for all four derivatives (Table 7), which indicates that the same mechanism is essentially operative. The computed large negative $\Delta S^{\ddagger}$ value implies that the rate-determining step involves the initial water association with the nitrosyl species.

Interaction of DNA with the Aqua Derivatives 5−8. Since ruthenium complexes encompassing polypyridyl-based ligands are known to participate in the DNA intercalation process,[23] the possibility of interaction of the present set of aqua complexes **5**−**8** with CT DNA (CT = calf thymus) was explored in TBS (pH 7.8) by using the fluorescence technique. All the complexes exhibited very weak to negligible emission in TBS at 298 K. In the presence of CTDNA in TBS, practically no enhancement of fluorescence intensity was observed for **5**, **6**, and **8**. However, in the case of **7**, the aqua derivative containing the 2-(2-pyridyl)-benzimidazole ligand (L^3), a substantial increase in intensity at 600 nm was observed in the presence of DNA (Figure 11). The intensity of emission at 600 nm kept increasing with the sequential enhancement of the complex concentration at a fixed concentration of DNA, and it leveled off at a ratio [**7**]:[DNA] = 1.4:1 (Figure 11). This indeed suggests the binding of **7** with DNA, which in turn stabilizes the excited states, resulting in enhanced emission.

The interaction of **7** with CT DNA was also followed via the spectroscopic titration of **7** with DNA in TBS at 298 K. Upon titration, small but significant changes were observed in the intensities of the Ru^{II}−trpy-based MLCT band (458 nm), as well as in the UV band at 310 nm (Figure 11, inset). The increase was 10% at the MLCT band and 19% at the 310 nm band. These enhancements are probably an implication of intercalation of **7** involving the stacking interaction

(23) (a) Pellegrini, P. P.; Aldrich-Wright, J. R.*Dalton Trans*. **2003**, 176. (b) Majumder, K.; Butcher, R. J.; Bhattacharya, S. *Inorg. Chem*. **2002**, *41*, 4605. (c) Swavey, S.; Brewer, K. J. *Inorg. Chem*. **2002**, *41*, 6196. (d) Chan, H.-L.; Liu, H.-Q.; Tzeng, B.-C.; You, Y.-S.; Peng, S.-M.; Yang, M.; Che, C.-M. *Inorg. Chem*. **2002**, *41*, 3161. (e) Patterson, B. T.; Collins, J. G.; Foley, F. M.; Keene, F. R. *J. Chem. Soc., Dalton Trans*. **2002**, 4343. (f) Frodl, A.; Herebian, D.; Sheldrick, W. S. *J. Chem. Soc., Dalton Trans*. **2002**, 3664. (g) Farrer, B. T.; Thorp, H. H. *Inorg. Chem*. **2000**, *39*, 44. (h) Ambroise, A.; Maiya, B. G. *Inorg. Chem*. **2000**, *39*, 4256. (i) Collins, J. G.; Sleeman, A. D.; Aldrich-Wright, J. R.; Greguric, I.; Hambley, T. W. *Inorg. Chem*. **1998**, *37*, 3133. (j) Cheng, C. C.; Goll, J. G.; Neyhart, G. A.; Walch, T. W.; Singh, P.; Thorp, H. H. *J. Am. Chem. Soc*. **1995**, *117*, 2970. (k) Novakova, O.; Kasparkova, J.; Vruna, O.; vanvliet, P. M.; Reedijk, J.; Brabec, V. *Biochemistry* **1995**, *34*, 12369. (l) Esposito, G.; Cauci, S.; Fogolari, F.; Alessio, E.; Scocchi, M.; Quadrifoglio, F.; Viglino, P. *Biochemistry* **1992**, *31*, 7094. (m) Jenkins, Y.; Barton, J. K. *J. Am. Chem. Soc*. **1992**, *114*, 8736. (n) Eriksson, M.; Leijon, M.; Hiort, C.; Norden, B.; Graeslund, A. *J. Am. Chem. Soc*. **1992**, *114*, 4933. (o) Mei, H. Y.; Barton, J. K. *Proc. Natl. Acad. Sci. U.S.A*. **1988**, *85* 1339.

Table 7. Rate Constants, Activation Parameters, and Equilibrium Constant Values for the Conversion Process of $[Ru^{II}(trpy)(L^{1-4})(NO^+)]^{3+} + H_2O \rightarrow [Ru^{II}(trpy)(L^{1-4})(NO_2)]^+ + 2H^+$ in Water

compd	$10^4k_{303}/s^{-1}$	$10^4k_{313}/s^{-1}$	$10^4k_{323}/s^{-1}$	$\Delta H^{\ddagger}$/kJ M^{-1}	$\Delta S^{\ddagger}$/J K^{-1} M^{-1}	K
13	4.7	14.0	26.9	60.7 (0.5)	−106.9 (1.9)	3.8
14	3.9	8.4	15.9	58.2 (0.7)	−118.1 (2.2)	3.7
16	1.1	2.3	4.3	53.1 (0.4)	−87.9 (1.7)	2.1
15	1.5 (323 K)	3.0 (333 K)	6.9(343 K)	71.2 (0.2)	−99.0 (0.9)	0.4

between the aromatic chromophore and the DNA base pair.[24] The relatively smaller change in the intensity of the trpy-based MLCT band as compared to the UV region band in the presence of DNA may suggest that the ancillary ligand L^3 in **7** is preferentially inserted between the base pairs of the DNA.

In electrophoresis experiments varying concentrations of **7** (0.06−0.40 mM) were incubated with the circular form of *p*-Bluescript SK DNA under conditions described in the Experimental Section and analyzed via 0.7% agarose gel electrophoresis (Figure 12). No gel-electrophoretic separation

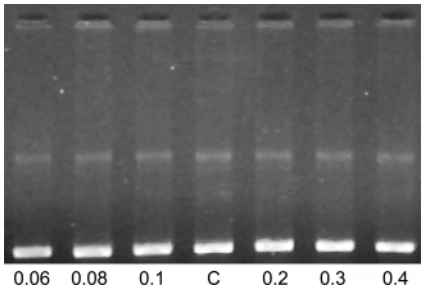

Figure 12. DNA interaction study for **7** by agarose gel electrophoresis using circular *p*-Bluescript DNA in TBE. Lane C is the DNA control with no metal complex added. The other lanes (left to right) are labeled with metal complex of different concentrations: 0.06, 0.08, 0.1, 0.2, 0.3, and 0.4 mM, respectively. Each of these lanes contains 100 ng of plasmid DNA.

of the *p*-Bluescript SK DNA was observed after incubation with **7**. The absence of additional bands corresponding to the relaxed coil or linear structure of DNA essentially suggests that, on binding with **7**, the DNA does not break into other forms. This was further confirmed via the UV-irradiation experiment where CT DNA in the presence of **7** in TBS was exposed to 254 nm light for 30 min and subsequently monitored by following the absorption spectra. No change in the spectral profile and intensity of the bands of **7** was observed on irradiation of both **7** and the mixture of **7** and DNA in TBS, indicating that the DNA is not damaged by the complex even on irradiation with UV light.

Conclusion

Depending on the electronic nature of the ancillary functionalities L^{1-4} as well as the isomeric structural forms **A** and **B**, the ν(NO) frequency of **13**−**16** varies substantially, 1957−1932 cm^{-1}, and it follows the order **13** ≫ **14** ≈ **15** > **16**. However, the $\{Ru^{II}(NO^+)\} \rightarrow \{Ru^{II}(NO^{\bullet})]^{2+}$ reduction potential follows a different trend: **14** > **13** ≫ **15** = **16**. Despite the appreciably high ν(NO) frequencies, particularly with **13**, for which the ν(NO) of 1957 cm^{-1} is rather higher than that of the bpy analogue (1952 cm^{-1}), the $\{Ru^{II}(NO^+)\} \rightarrow \{Ru^{II}(NO_2)\}$ transformation exhibits a slow-rate process ($k \approx 10^{-4}$ s^{-1}) and low equilibrium constant values (K = 0.4−3.8) even in aqueous medium. The chloro, aqua, and nitro derivatives exhibit moderately strong emissions at 77 K, $\phi = 5.76 \times 10^{-2}$ to 2.73×10^{-1}, and for a particular L, NO_2^- > H_2O > Cl^-. The aqua species **7** incorporating benzimidazole-derived L^3 selectively interacts with the DNA bases.

Experimental Section

The precursor complex $Ru^{III}(trpy)Cl_3$ was prepared as reported.[25] 2-(2-Pyridyl)benzimidazole (L^3) was purchased from Aldrich. 2-(2-Pyridyl)benzoxazole (L^1), 2-(2-pyridyl)benzothiazole (L^2), and 1-methyl-2-(2-pyridyl)-1*H*-benzimidazole (L^4) ligands were prepared by following the reported procedures.[26] Water of high purity was obtained by distillation of deionized water from $KMnO_4$ (pH 6.9). Other chemicals and solvents were reagent grade and used as received. For spectroscopic and electrochemical studies HPLC-grade solvents were used. Solution electrical conductivity was checked using a Systronic conductivity bridge 305. Infrared spectra were taken on a Nicolet spectrophotometer with samples prepared as KBr pellets. ^{1}H NMR spectra were recorded in $(CD_3)_2SO$ using a 300 MHz Varian FT spectrometer. UV−vis spectral studies were performed on a Jasco-570 spectrophotometer. Cyclic voltammetric and coulometric measurements were carried out using a PAR model 273A electrochemistry system. A platinum wire working electrode, a platinum wire auxiliary electrode, and a saturated calomel reference electrode (SCE) were used in a standard three-electrode configuration. Tetraethylammonium perchlorate (TEAP) was the supporting electrolyte, and the solution concentration of the analyte was ca. 10^{-3} M; the scan rate used was 50 mV s^{-1}. A platinum gauze working electrode was used in the coulometric experiments. All electrochemical experiments were carried out under a dinitrogen atmosphere. The EPR measurements were made with a Varian model 109C E-line X-band spectrometer fitted with a quartz dewar for measurements at 77 K. The elemental analyses were carried out with a Perkin-Elmer 240C elemental analyzer. Electrospray mass spectra were recorded on a Micromass Q-ToF mass spectrometer. Steady-state emission experiments were made using a Perkin-Elmer LS 55 luminescence spectrometer fitted with a cryostat. The florescence quantum yield was determined with reference to the standard complex $Ru(bpy)_3^{2+}$ following a reported method.[21]

Preparation of Complexes $[Ru^{II}(trpy)(L^{1-4})(Cl)]ClO_4$ (1−4), $[Ru^{II}(trpy)(L^{1-4})(H_2O)](ClO_4)_2$ (5−8), $[Ru^{II}(trpy)(L^{1-4})(NO_2)]ClO_4$ (9−12), and $[Ru^{II}(trpy)(L^{1,2,4})(NO)](ClO_4)_3$ (13, 14, 16)/$[Ru^{II}(trpy)(L^3)(NO)](ClO_4)_2(NO_3)$ (15). The complexes were prepared by following general procedures. The details are given for one set of complexes (1, 5, 9, and 13) having a 2-(2-pyridyl)benzoxazole ancillary ligand (L^1).

(24) Liu, F.; Wang, K.; Bai, G.; Zhang, Y.; Gao, L. *Inorg. Chem.* **2004**, *43*, 1799.

(25) Indelli, M. T.; Bignozzi, C. A.; Scandola, F.; Collin, J.-P. *Inorg. Chem.* **1998**, *37*, 6084.

(26) (a) Mansingh, P. S.; Mohanty, R. R.; Jena, S.; Dash, K. C. *Indian J. Chem.* **1996**, *35A*, 479. (b) Addison, A. W.; Rao, T. N.; Wahlgren, C. G. *J. Heterocycl. Chem.* **1983**, *20*, 1481.

Synthesis of $[Ru^{II}(trpy)(L^1)(Cl)]ClO_4$ (1). $[Ru^{III}(trpy)Cl_3]$ (100 mg, 0.23 mmol), 2-(2-pyridyl)benzoxazole ligand (L^1; 54 mg, 0.28 mmol), excess LiCl (54 mg, 1.3 mmol), and NEt_3 (0.4 mL) were taken in 20 mL of methanol, and the mixture was heated at reflux for 3 h under a dinitrogen atmosphere. The solution gradually changed to deep purple-red. The solvent was then removed under reduced pressure. The dry mass was dissolved in a minimum volume of acetonitrile, and an excess saturated aqueous solution of $NaClO_4$ was added to it. The solid precipitate thus formed was filtered off and washed thoroughly with ice-cold water. The product was dried in vacuo over P_4O_{10}. It was then purified by using a silica gel column. Complex **1** was eluted by 4:1 $CH_2Cl_2-CH_3CN$. Evaporation of the solvent under reduced pressure afforded pure complex **1**. Yield: 116 mg (77%). Anal. Calcd (Found): C, 48.73 (48.39); H, 2.88 (2.90); N, 10.52 (10.43). Molar conductivity [Λ_M (Ω^{-1} cm^2 M^{-1})] in acetonitrile: 140. λ_{max}/nm (ϵ/M^{-1} cm^{-1}) in acetonitrile: 516 (10320), 316 (45700), 274 (23390), 234 (30415), 198 (50225). The electrospray mass spectrum in acetonitrile showed the molecular ion peak centered at m/z = 566.05 corresponding to $[\mathbf{1} - ClO_4]^+$ (calculated molecular mass 566.03). ^{1}H NMR (δ/ppm (J/Hz), DMSO-d_6): 8.88 (t, 6.2/6.8); 8.84 (d, 7.4); 8.70 (d, 7.5); 8.46 (d, 7.4); 8.26 (m); 8.04 (m); 7.88 (m); 7.76 (t, 6.0); 7.46 (d, 6.0); 7.38 (t, 6.0); 7.22 (t, 6.0).

Data for $[Ru^{II}(trpy)(L^2)(Cl)]ClO_4$ (2). Yield: 96 mg (62%). Anal. Calcd (Found): C, 47.58 (47.24); H, 2.81 (2.84); N, 10.28 (10.66). Molar conductivity [Λ_M (Ω^{-1} cm^2 M^{-1})] in acetonitrile: 160. λ_{max}/nm (ϵ/M^{-1} cm^{-1}) in acetonitrile: 524 (9980), 316 (37015), 274 (20040), 232 (28970), 200 (44700). The electrospray mass spectrum in acetonitrile showed the molecular ion peak centered at m/z = 581.94 corresponding to $[\mathbf{2} - ClO_4]^+$ (calculated molecular mass 582.01). ^{1}H NMR (δ/ppm (J/Hz), DMSO-d_6): 8.92 (d, 5.1); 8.70 (d, 5.6); 8.43 (t, 4.5/4.7); 8.34 (t, 4.8/5.1); 8.18 (d, 5.7); 8.13 (t, 4.2/4.5); 7.95 (t, 4.5/5.1); 7.65 (d, 3.4); 7.43 (d, 5.4); 7.35 (t, 4.2/4.5); 7.20 (t, 5.7/5.1).

Data for $[Ru^{II}(trpy)(L^3)(Cl)]ClO_4$ (3). Yield: 104 mg (69%). Anal. Calcd (Found): C, 48.81 (48.46); H, 3.03 (3.05); N, 12.65 (12.33). Molar conductivity [Λ_M (Ω^{-1} cm^2 M^{-1})] in acetonitrile: 160. λ_{max}/nm (ϵ/M^{-1} cm^{-1}) in acetonitrile: 520 (7400), 318 (38860), 272 (20390), 240 (32380), 200 (43140). The electrospray mass spectrum in acetonitrile showed the molecular ion peak centered at m/z = 564.98 corresponding to $[\mathbf{3} - ClO_4]^+$ (calculated molecular mass 565.05). ^{1}H NMR (δ/ppm (J/Hz), DMSO-d_6): 8.92 (d, 9.0); 8.77 (d, 9.0); 8.66 (d, 9.0); 8.35 (d, 9.0); 8.14 (t, 8.6); 7.94 (t, 9.0); 7.82 (t, 8.1); 7.76 (d, 6.0); 7.62 (t, 9.0); 7.48 (t, 7.8); 7.35 (t, 7.5); 7.25 (d, 6.0); 7.04 (t, 7.5).

Data for $[Ru^{II}(trpy)(L^4)(Cl)]ClO_4$ (4). Yield: 115 mg (75%). Anal. Calcd (Found): C, 49.57 (49.83); H, 3.27 (3.08); N, 12.39 (12.01). Molar conductivity [Λ_M (Ω^{-1} cm^2 M^{-1})] in acetonitrile: 150. λ_{max}/nm (ϵ/M^{-1} cm^{-1}) in acetonitrile: 514 (9426), 318 (43330), 272 (23960), 236 (34400). The electrospray mass spectrum in acetonitrile showed the molecular ion peak centered at m/z = 578.93 corresponding to $[\mathbf{4} - ClO_4]^+$ (calculated molecular mass 579.06). ^{1}H NMR (δ/ppm (J/Hz), DMSO-d_6): 9.08 (d, 9.0); 8.78 (d, 9.0); 8.66 (d, 9.0); 8.52 (d, 9.0); 8.15 (t, 9.4); 7.94 (t, 7.4/6.9); 7.74 (m); 7.50 (t, 9.0); 7.36 (m); 7.06 (t, 7.5).

Synthesis of $[Ru^{II}(trpy)(L^1)(H_2O)](ClO_4)_2$ (5). The chloro complex **1** (100 mg, 0.15 mmol) was taken in 20 mL of water and heated at reflux for 5 min. An excess of $AgNO_3$ (255 mg, 1.5 mmol) was added to the above hot solution, and heating was continued for 1 h. It was then cooled, and the precipitated AgCl was separated by filtration through a sintered glass crucible (G-4). The volume of the filtrate was reduced to 10 mL, and saturated aqueous $NaClO_4$ solution was added. The solid aqua complex **5** thus obtained was filtered off, washed with ice-cold water, and dried in vacuo over P_4O_{10}. Yield: 92 mg (82%). Anal. Calcd (Found): C, 43.39 (43.10); H, 2.83 (2.86); N, 9.37 (9.29). Molar conductivity [Λ_M (Ω^{-1} cm^2 M^{-1})] in water: 205. λ_{max}/nm (ϵ/M^{-1} cm^{-1}) in acetonitrile: 458 (8705), 330 (21275), 304 (43740), 274 (21585), 202 (39270). The electrospray mass spectrum in water showed the molecular ion peak centered at m/z = 629.99 corresponding to $[\mathbf{5} - H_2O - ClO_4]^+$ (calculated molecular mass 630.01). ^{1}H NMR (δ/ppm (J/Hz), DMSO-d_6): 8.51 (d, 9.2); 8.28 (d, 9.4); 7.78 (m); 7.84 (t, 9.0); 7.72 (d, 7.5); 7.52 (d, 9.5); 7.28 (d, 8.2); 7.20 (t, 8.4/8.2); 6.96 (t, 9.1/9.3).

Data for $[Ru^{II}(trpy)(L^2)(H_2O)](ClO_4)_2$ (6). Yield: 88 mg (79%). Anal. Calcd (Found): C, 42.47 (42.21); H, 2.77 (2.79); N, 9.17 (9.10). Molar conductivity [Λ_M (Ω^{-1} cm^2 M^{-1}] in water: 220. λ_{max}/nm (ϵ/M^{-1} cm^{-1}) in acetonitrile: 468 (6570), 308 (29800), 274 (16160), 202 (40250). The electrospray mass spectrum in water showed the molecular ion peak centered at m/z = 644.22 corresponding to $[\mathbf{6} - H_2O - ClO_4]^+$ (calculated molecular mass 645.99). ^{1}H NMR (δ/ppm (J/Hz), DMSO-d_6): 8.74 (d, 6.2); 8.65 (d, 6.0); 8.58 (d, 6.0); 8.40 (m); 8.30 (d, 6.2); 7.95 (d, 6.2); 7.83 (m); 7.72 (d, 5.6); 7.40 (d, 5.2); 7.25 (t, 4.8/4.6); 7.05 (t, 5.4/5.2).

Data for $[Ru^{II}(trpy)(L^3)(H_2O)](ClO_4)_2$ (7). Yield: 98 mg (87%). Anal. Calcd (Found): C, 43.44 (43.10); H, 2.97 (3.00); N, 11.26 (10.94). Molar conductivity [Λ_M (Ω^{-1} cm^2 M^{-1})] in water: 210. λ_{max}/nm (ϵ/M^{-1} cm^{-1}) in acetonitrile: 458 (7460), 310 (41360), 274 (19920), 202 (50780). The electrospray mass spectrum in water showed the molecular ion peak centered at m/z = 627.99 corresponding to $[\mathbf{7} - H_2O - ClO_4]^+$ (calculated molecular mass 629.03). ^{1}H NMR (δ/ppm (J/Hz), DMSO-d_6): 8.57 (d, 9.6); 8.42 (d, 9.2); 8.22 (m); 7.96 (m); 7.80 (d, 9.0); 7.72 (t, 9.0); 7.62 (t, 9.2); 7.31 (d, 7.8); 7.25 (t, 7.8); 7.02 (t, 7.6).

Data for $[Ru^{II}(trpy)(L^4)(H_2O)](ClO_4)_2$ (8). Yield: 95 mg (85%). Anal. Calcd (Found): C, 44.22 (44.58); H, 3.18 (3.51); N, 11.05 (10.79). Molar conductivity [Λ_M (Ω^{-1} cm^2 M^{-1})] in water: 225. λ_{max}/nm (ϵ/M^{-1} cm^{-1}) in acetonitrile: 460 (8990), 308 (41315), 272 (19180). The electrospray mass spectrum in water showed the molecular ion peak centered at m/z = 643.13 corresponding to $[\mathbf{8} - H_2O - ClO_4]^+$ (calculated molecular mass 643.04). ^{1}H NMR (δ/ppm (J/Hz), DMSO-d_6): 8.58 (d, 9.0); 8.42 (d, 9.2); 8.24 (m); 7.94 (t, 8.4); 7.78 (m); 7.72 (d, 6.6); 7.64 (t, 9.0/8.7); 7.40 (d, 8.5); 7.26 (m); 7.03 (t, 7.7/7.6).

Synthesis of $[Ru^{II}(trpy)(L^1)(NO_2)]ClO_4$ (9). The aqua complex **5** (100 mg, 0.13 mmol) was dissolved in 20 mL of hot water, and an excess of $NaNO_2$ (92 mg, 1.34 mmol) was added to it. The mixture was heated at reflux for 2 h. The red-brown solution of the aqua species changed to orange during the course of reaction. The pure crystalline nitro complex was precipitated out when the hot solution cooled to room temperature. The solid mass thus obtained was filtered off, washed with ice-cold water, and dried in vacuo over P_4O_{10}. Yield: 72 mg (80%). Anal. Calcd (Found): C, 47.97 (48.25); H, 2.83 (2.80); N, 12.43 (12.50). Molar conductivity [Λ_M (Ω^{-1} cm^2 M^{-1})] in acetonitrile: 130. λ_{max}/nm (ϵ/M^{-1} cm^{-1}) in acetonitrile: 480 (6884), 310 (34450), 272 (19700), 200 (52525). The electrospray mass spectrum in acetonitrile showed the molecular ion peak centered at m/z = 577.06 corresponding to $[\mathbf{9} - ClO_4]^+$ (calculated molecular mass 577.06). ^{1}H NMR (δ/ppm (J/Hz), DMSO-d_6): 8.94 (d, 11.1); 8.78 (d, 11.4); 8.53 (d, 11.4); 8.46 (d, 12.0); 8.34 (d, 11.6); 8.20 (d, 11.4); 8.12 (d, 11.0); 8.06 (t, 10.7/11.0); 7.92 (t, 10.2/10.5); 7.81 (t, 10.5/10.8); 7.50 (d, 7.5); 7.42 (t, 9.6/9.4); 7.33 (t, 9.0/9.2).

Data for $[Ru^{II}(trpy)(L^2)(NO_2)]ClO_4$ (10). Yield: 65 mg (72%). Anal. Calcd (Found): C, 46.86 (47.21); H, 2.77 (2.75); N, 12.14 (12.22). Molar conductivity [Λ_M (Ω^{-1} cm^2 M^{-1})] in acetonitrile:

132. λ_{max}/nm (ϵ/M^{-1} cm^{-1}) in acetonitrile: 484 (8700), 310 (40600), 274 (22500), 202 (58640). The electrospray mass spectrum in acetonitrile showed the molecular ion peak centered at $m/z = 593.13$ corresponding to $[\mathbf{10} - ClO_4]^+$ (calculated molecular mass 593.03). ^{1}H NMR (δ/ppm (J/Hz), DMSO-d_6): 9.02 (d, 6.0); 8.91 (d, 6.0); 8.82 (t, 5.4/5.7); 8.77 (d, 6.0); 8.68 (m); 8.21 (t, 5.4/5.7); 8.13 (d, 6.0); 8.04 (m); 7.78 (m); 7.50 (d, 5.7); 7.42 (t, 4.8/4.9); 7.21 (t, 5.8/5.6).

Data for $[Ru^{II}(trpy)(L^3)(NO_2)]ClO_4$ (11). Yield: 70 mg (78%). Anal. Calcd (Found): C, 48.04 (48.42); H, 2.99 (3.01); N, 14.52 (14.12). Molar conductivity [Λ_M (Ω^{-1} cm^2 M^{-1})] in acetonitrile: 128. λ_{max}/nm (ϵ/M^{-1} cm^{-1}) in acetonitrile: 480 (7820), 314 (45815), 272 (24615), 200 (59925). The electrospray mass spectrum in acetonitrile showed the molecular ion peak centered at $m/z = 575.95$ corresponding to $[\mathbf{11} - ClO_4]^+$ (calculated molecular mass 576.07). ^{1}H NMR (δ/ppm (J/Hz), DMSO-d_6): 8.80 (d, 6.2); 8.72 (d, 5.9); 8.56 (t, 6.0); 8.30 (t, 6.0/5.8); 8.05 (t, 5.7/5.9); 7.86 (m); 7.73 (t, 5.4/5.9); 7.58 (d, 4.5); 7.44 (t, 4.7/4.9); 7.38 (t, 4.4/4.6); 7.23 (m); 7.00 (d, 4.6); 6.93 (t, 4.6/4.5).

Data for $[Ru^{II}(trpy)(L^4)(NO_2)]ClO_4$ (12). Yield: 75 mg (83%). Anal. Calcd (Found): C, 48.81 (49.13); H, 3.22 (3.44); N, 14.23 (14.55). Molar conductivity [Λ_M (Ω^{-1} cm^2 M^{-1})] in acetonitrile: 145. λ_{max}/nm (ϵ/M^{-1} cm^{-1}) in acetonitrile: 476 (9000), 312 (43215), 268 (21980). The electrospray mass spectrum in acetonitrile showed the molecular ion peak centered at $m/z = 590.12$ corresponding to $[\mathbf{12} - ClO_4]^+$ (calculated molecular mass 590.09). ^{1}H NMR (δ/ppm (J/Hz), DMSO-d_6): 8.87 (d, 6.2); 8.80 (d, 6.2); 8.64 (d, 6.0); 8.42 (t, 5.8/6.0); 8.28 (t, 6.0); 8.16 (d, 6.4); 7.97 (m); 7.72 (d, 4.8); 7.50 (t, 6.0/6.2); 7.43 (d, 4.8); 7.38 (t, 5.8/5.6); 7.20 (t, 5.4/5.6).

Synthesis of $[Ru^{II}(trpy)(L^1)(NO)](ClO_4)_3$ (13). Concentrated HNO_3 (2 mL) was added dropwise directly to the solid nitro complex **9** (100 mg, 0.15 mmol) at 273 K under stirring conditions. To the pasty mass thus formed was added ice-cold concentrated $HClO_4$ (6 mL) dropwise with continuous stirring by using a glass rod. A yellow solid product was formed on addition of saturated aqueous $NaClO_4$ solution. The precipitate was filtered off immediately, washed with a little ice-cold water, and then dried in vacuo over P_4O_{10}. Yield: 114 mg (90%). Anal. Calcd (Found): C, 37.76 (38.10); H, 2.23 (2.24); N, 9.78 (9.83). Molar conductivity [Λ_M (Ω^{-1} cm^2 M^{-1})] in acetonitrile: 340. λ_{max}/nm (ϵ/M^{-1} cm^{-1}) in acetonitrile: 366 (7640), 316 (22460), 228 (30390), 202 (45240). The electrospray mass spectrum in acetonitrile showed the molecular ion peak centered at $m/z = 759.96$ [Supporting Information (Figure S3)] corresponding to $[\mathbf{13} - ClO_4]^+$ (calculated molecular mass 758.96). ^{1}H NMR (δ/ppm (J/Hz), DMSO-d_6): 9.22 (d, 7.4); 9.02 (d, 9.0); 8.82 (d, 9.0); 8.67 (d, 9.2); 8.50 (m); 8.34 (d, 9.2); 8.23 (t, 9.0); 8.03 (d, 7.6); 7.51 (d, 7.2); 7.38 (t, 8.2/8.0); 7.33 (t, 6.9/7.2).

Data for $[Ru^{II}(trpy)(L^2)(NO)](ClO_4)_3$ (14). Yield: 104 mg (82%). Anal. Calcd (Found): C, 37.06 (37.36); H, 2.19 (2.21); N, 9.60 (9.53). Molar conductivity [Λ_M (Ω^{-1} cm^2 M^{-1})] in acetonitrile: 340. λ_{max}/nm (ϵ/M^{-1} cm^{-1}) in acetonitrile: 384 (8570), 320 (23970), 226 (42700), 200 (64870). The electrospray mass spectrum in acetonitrile showed the molecular ion peak centered at $m/z = 776.09$ [Supporting Information (Figure S3)] corresponding to $[\mathbf{14} - ClO_4]^+$ (calculated molecular mass 774.93). ^{1}H NMR (δ/ppm (J/Hz), DMSO-d_6): 9.55 (d, 5.8); 9.27 (m); 9.15 (d, 7.2); 9.00 (d, 6.9); 8.80 (t, 7.5/7.3); 8.53 (t, 7.8/7.5); 8.42 (t, 7.2/7.4); 8.14 (d, 5.6); 7.82 (t, 6.0); 7.57 (t, 6.6/6.8); 7.42 (m); 7.34 (t, 7.0/7.2).

Data for $[Ru^{II}(trpy)(L^3)(NO)](ClO_4)_2(NO_3)$ (15). Yield: 107 mg (88%). Anal. Calcd (Found): C, 39.51 (39.29); H, 2.46 (2.51); N, 13.66 (13.74). Molar conductivity [Λ_M (Ω^{-1} cm^2 M^{-1})] in acetonitrile: 346. λ_{max}/nm (ϵ/M^{-1} cm^{-1}) in acetonitrile: 365 (19810), 346 (24800), 284 (16030), 232 (44530), 202 (70300). The electrospray mass spectrum in acetonitrile showed the molecular ion peak centered at $m/z = 657.97$ [Supporting Information (Figure S3)] corresponding to $[\mathbf{15}$ (incorporating $NO^{\bullet}$) $- ClO_4 - NO_3]^+$ (calculated molecular mass 659.02). ^{1}H NMR (δ/ppm (J/Hz), DMSO-d_6): 9.22 (d, 6.0); 9.12 (d, 6.0); 9.02 (d, 6.2); 8.54 (t, 7.2/6.9); 8.34 (t, 6.2/6.0); 8.14 (m); 8.04 (m); 7.94 (d, 5.6); 7.78 (d, 6.0); 7.62 (m); 7.42 (t, 6.0); 7.29 (d, 6.2).

Data for $[Ru^{II}(trpy)(L^4)(NO)](ClO_4)_3$ (16). Yield: 102 mg (81%). Anal. Calcd (Found): C, 38.57 (38.78); H, 2.54 (2.66); N, 11.24 (11.57). Molar conductivity [Λ_M (Ω^{-1} cm^2 M^{-1})] in acetonitrile: 350. λ_{max}/nm (ϵ/M^{-1} cm^{-1}) in acetonitrile: 400 (7000), 322 (32600), 284 (27850), 230 (40250), 208 (49750). The electrospray mass spectrum in acetonitrile showed the molecular ion peak centered at $m/z = 771.23$ [Supporting Information (Figure S3)] corresponding to $[\mathbf{16} - ClO_4]^+$ (calculated molecular mass 771.99). ^{1}H NMR (δ/ppm (J/Hz), DMSO-d_6): 9.23 (d, 7.5); 9.14 (d, 7.2); 9.04 (d, 7.2); 8.88 (d, 7.8); 8.54 (t, 7.5/7.2); 8.43 (t, 7.5); 8.36 (d, 7.6); 8.23 (d, 7.5); 8.02 (d, 6.0); 7.84 (m); 7.76 (t, 6.9/6.6); 7.56 (t, 6.2); 7.48 (d, 6.0).

Kinetic Measurements. For the determination of k of the conversion process $[Ru^{II}(trpy)(L)(NO)]^{3+} \rightarrow [Ru^{II}(trpy)(L)(NO_2)]^+$ in water, the increase in absorbance (A_t) corresponding to λ_{max} of the nitro derivative was monitored as a function of time (t). A_α was measured when the intensity changes leveled off. Values of pseudo-first-order rate constants, k, were obtained from the slopes of linear least-squares plots of $-\ln(A_\alpha - A_t)$ against t. The activation parameters $\Delta H^{\ddagger}$ and $\Delta S^{\ddagger}$ were determined from the Eyring plot.[27]

DNA Interaction. The interaction of circular *p*-Bluescript DNA with complex **7** was analyzed by agarose gel electrophoresis as previously described.[23,28] The concentration of the DNA was determined by staining with ethidium bromide and observation on a UV illuminator. In a typical experiment 4 μL of *p*-Bluescript DNA (100ng) was incubated in an Eppendorf tube with 18 μL of metal complex of different concentrations (0.06, 0.08, 0.1, 0.2, 0.3, and 0.4 mM) in TBE solution. The samples were incubated for 30 min at 25 °C, and 22 μL was analyzed via 0.7% agarose electrophoresis. The gels were then stained with 0.5 μg/mL ethidium bromide for 1 h and documented with UV illumination using a KDs120 gel documentation system from Kodak Digital Science.

Crystal Structure Determination. Single crystals of **1**, **2**, **4**, **9**, **12**, **13**, **15**, and **16** were grown by slow diffusion of an acetonitrile solution of the complex in benzene followed by slow evaporation. The X-ray data for **1**, **4**, **9**, and **12** and **2**, **13**, **15**, and **16** were collected on PC-controlled Enraf-Nonius CAD-4 (MACH-3) and on Bruker SMART APEX CCD single-crystal X-ray diffractometers, respectively. The structures were solved and refined by full-matrix least-squares techniques on F^2 using SHELX-97 (SHELXTL program package).[29] All the data were corrected for Lorentz, polarization, and absorption effects. X-ray analysis revealed that in **2** there are two complex molecules along with half of a distorted methanol molecule of crystallization in the asymmetric unit. Similarly, in **13** there are two complex molecules along with one and a half distorted acetonitrile molecules of crystallization in the asymmetric unit. The asymmetric unit of **9**,

(27) Wilkins, R. G. *The study of kinetics and mechanism of reaction of Transition Metal Complexes*; Allyn and Bacon: Boston, MA, 1974.
(28) Kar, S.; Pradhan, B.; Sinha, R. K.; Kundu, T.; Kodgire, P.; Rao, K. K.; Puranik, V. G.; Lahiri, G. K. *Dalton Trans.* **2004**, 1752.
(29) Sheldrick, G. M. *Program for Crystal Structure Solution and Refinement*; Universität Göttingen: Göttingen, Germany, 1997.

15, and **16** contains $0.5H_2O$, H_2O/C_6H_6 (1:0.5), and $2H_2O$ of crystallization, respectively.

Acknowledgment. This paper is dedicated to Professor Animesh Chakravorty on the occasion of his 70th birthday. We thank the Department of Science and Technology and Council of Scientific and Industrial Research, New Delhi, India, for financial support. The X-ray structural studies were carried out at the National Single Crystal Diffractometer Facility, Indian Institute of Technology—Bombay. Special acknowledgment is made to the Sophisticated Analytical Instrument Facility, Indian Institute of Technology—Bombay, for providing the NMR and EPR facilities.

Supporting Information Available: X-ray crystallographic data for **1**, **2**, **4**, **9**, **12**, **13**, **15**, and **16** in CIF format and ORTEP diagrams of **4**, **9**, and **12** (Figures S1−S3), ν(NO) frequencies of **13**−**16** (Figure S4), ^{1}H NMR spectra of **1**−**4** in $(CD_3)_2SO$ (Figure S5), and electrospray mass spectra of **13**−**16** (Figure S6) (PDF). This material is available free of charge via the Internet at http://pubs.acs.org.

IC048184W